11/28/2022   Earthquake Sources

Earthquakes are primarily caused by spontaneous dynamic slippage on a surface in the Earth (a fault). It turns out to be quite difficult to solve elasticity problems in which there is an arbitrary cut in the medium (a slipping fault). One common approach is to create a finite-element model of the volume that contains the fault slippage. Brad Aagaard's PhD thesis has an excellent description of this problem (Finite-element simulations of earthquakes, Aagaard, B, 1999, Finite-element simulations of earthquakes. EERL Report, 99-03. California Institute of Technology , Pasadena, CA., https://resolver.caltech.edu/CaltechEERL:1999.EERL-99-03).

Specialized elements that have split nodes create lateral offsets within the finite element grid. Except for these specialized split elements, all other elements are assumed to deform elastically. The slips at the fault elements can be determined in two ways, 1) the slip vector can be prescribed as a function of location and time (this is usually called a kinematic source), or 2) a prestress and a friction law is prescribed, and the slip vector is calculated (this is called a dynamic source model). Since both modeling approaches obey the laws of linear continuum mechanics, the motions that occur in their volumes are identical as long as the slip time histories are the same.

One of the difficulties with kinematic sources is that the modeler can choose slip vectors that are inconsistent with classical dynamics; for instance, one could choose a slip that reverses direction, or a slip that jumps instantaneously from one position to another. It is up to the modeler to decide what slip distribution is reasonable.

In contrast, dynamic models use the continuum equations to determine the slip history and therefore, they are often referred to as physics-based models. Of course, there is no free lunch; that is, the modeler must specify the prestress and the friction law. I will argue in Chapter 8 that neither of these quantities are known. Furthermore, dynamic modeling is considerably more difficult to interpret, and it is computationally expensive. Therefore, there are many applications that are more efficient using kinematic models. This is particularly true for source inversions, where the object is to find source slip histories that best simulate recorded seismic information. Seismograms are linear functions of slip, whereas they are highly nonlinear functions of prestress and friction. Linear inversions are typically fast, and more importantly, their solutions are unique.

Although finite element models are versatile, they can be cumbersome for problems with large spatial domains.   There have been attempts to extend the domain of finite-element solutions by using the motions on the boundary of the discrete domain as boundary conditions for analytic solutions, but that subject is beyond the scope of this class.

Seismologists simulated earthquakes decades before the advent of finite-element modeling. My favorite papers on this topic were both printed in the same 1964 issue of the Bulletin of the Seismological Society of America. Haskell (1964) described a method to simulate the far-field waves from dislocations (a truly profound paper), and Burridge and Knopoff (1964) described how different types of seismic sources could be simulated using equivalent forces. Reading these early papers provides the background to understand the meaning of the terms used in earthquake studies.

It is important to understand that researchers sought a methodology to modify known solutions to continuum mechanics so that they simulate earthquakes. An important example is shown in Figure 7.1.
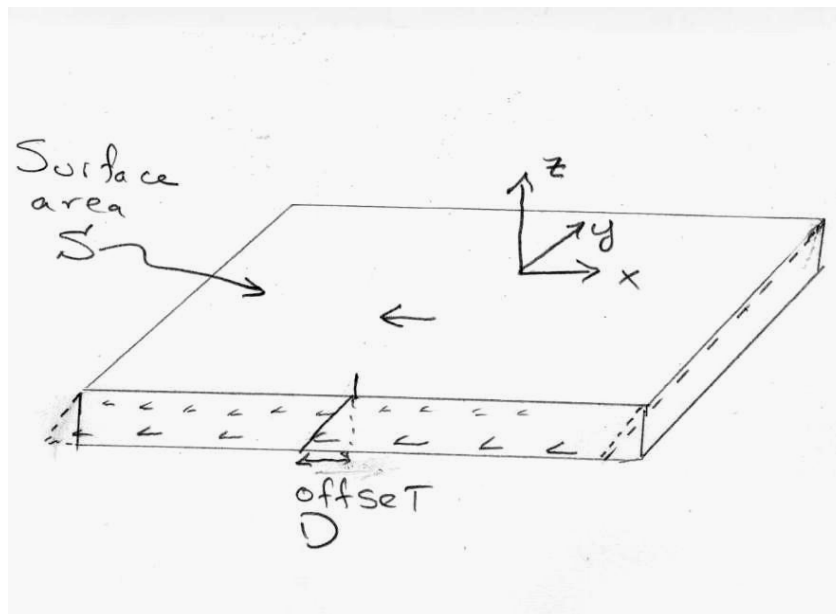

Figure 7.1 Mathematical idealization of an "earthquake fault." In this case we have an elastic material in which we induce a shear strain inside a tabular body. The opposing surfaces of the tabular body are offset by the induced shear strain. We then shrink the thickness of the tabular body to zero, but increase the shear strain so that the net offset is constant; that is, we make the shear strain an impulse in the z-coordinate.

It is usually assumed that the Earth is linearly elastic everywhere, except in the immediate vicinity of the failure surface. It is very difficult to find analytic equations to a continuum that has a surface with discontinuous displacement (fault slip). To find analytic solutions, it is convenient to draw a tabular box around the failure surface as is shown in Figure 7.1. In fact, it is usually far easier to solve problems in which we apply stresses in such a manner that the medium deforms "as if" it had a cut along some plane. Now if strains are small and if the material is isotropic, then the strain anywhere in the medium can be related to stress by

$$\varepsilon_{ij} = \frac{1+\nu}{E}\sigma_{ij} - \frac{\nu}{E}\delta_{ij}\sum_{k=1}^{3}\sigma_{kk} \tag{7.1}$$

where ν and E are Poisson's ratio and Young's modulus, respectively. We can also write (7.1) in terms of the Lame constants, where

$$\nu = \frac{\lambda}{2(\lambda+\mu)} \tag{7.2}$$

$$E = \frac{\mu(3\lambda+2\mu)}{\lambda+\mu} \tag{7.3}$$

A little algebra gives

$$\varepsilon_{ij} = \frac{1}{2\mu}\sigma_{ij} - \frac{\lambda}{2\mu(3\lambda+2\mu)}\delta_{ij}\sum_{k=1}^{3}\sigma_{kk} \tag{7.4}$$

Now if we were God, then we could apply a stress $\boldsymbol{\sigma}^0(x,y,z)$ within the tabular box. Now the stress at any point inside the box will be the sum of the stress that we applied at that point $\boldsymbol{\sigma}^0(x,y,z)$ plus the stresses $\hat{\boldsymbol{\sigma}}^0$ at (x,y,z) that are caused by application of stress $\boldsymbol{\sigma}^0(\hat{x}\neq x,\hat{y}\neq y,\hat{z}\neq z)$ at all other points than (x,y,z). That is, the stress anywhere in the medium can be decomposed as

$$\boldsymbol{\sigma}(x,y,z) = \boldsymbol{\sigma}^0(x,y,z) + \hat{\boldsymbol{\sigma}}^0(x,y,z) \tag{7.5}$$

The terms $\hat{\boldsymbol{\sigma}}^0(x,y,z)$ are actually very complex and, for each point in space, they involve integrating Green's functions for stress over the entire box. However, we will assume that our box becomes vanishingly thin. In fact, we will assume that

$$\boldsymbol{\sigma}^0(x,y,z) = \boldsymbol{\sigma}^0(x,y,0)\delta(z) \tag{7.6}$$

where $\delta(z)$ is an impulse function in z. Now as it turns out, the Green's function for stress at (x,y,z) caused by applying another stress at $(\hat{x},\hat{y},\hat{z})$ is a complex function with a scaling of $|\sigma|\sim r^{-3} = \left[(x-\hat{x})^2+(y-\hat{y})^2+(z-\hat{z})^2\right]^{-3/2}$. This means that if (7.6) is true, then within the box, the stresses are completely dominated by the impulsive stress applied at each point within the box (that is, stress decays as the inverse cube of the distance from the point at which the stress is applied) and

$$\boldsymbol{\sigma}(x,y,z\approx 0) \approx \boldsymbol{\sigma}^0(x,y,0)\delta(z) \tag{7.7}$$

3

Now if we are interested in the relative displacement vector $\mathbf{D}^z$ of the two opposite faces (perpendicular to the z direction) of the tabular box, then we can integrate the strain from one side of the box to the other. The strain in the box is just

$$\varepsilon^0{}_{ij} \approx \frac{1}{2\mu}\sigma^0_{ij}(x,y)\delta(z) - \frac{\lambda}{2\mu(3\lambda+2\mu)}\delta_{ij}\sum_{k=1}^{3}\sigma^0_{kk}(x,y)\delta(z) \qquad (7.8)$$

Since we are interested in the jump in displacement $\mathbf{D}(x,y)$ that occurs from the top to the bottom of the box, we can write that

$$D_x(x,y) = \int_{-\varepsilon}^{+\varepsilon} 2\varepsilon_{xz}(xy)\,dz = \frac{\sigma^0_{xz}}{\mu}$$

$$D_y(x,y) = \int_{-\varepsilon}^{+\varepsilon} 2\varepsilon_{yz}(xy)\,dz = \frac{\sigma^0_{xy}}{\mu}$$

$$\qquad (7.9)$$

$$D_z(x,y) = \int_{-\varepsilon}^{+\varepsilon} \varepsilon_{zz}(xy)\,dz = \frac{1}{2\mu}\sigma^0_{zz}(x,y) - \frac{\lambda}{2\mu(3\lambda+2\mu)}\sum_{k=1}^{3}\sigma^0_{kk}(x,y)$$

$$= \frac{\sigma^0_{zz}(x,y) - v\sigma^0_{xx}(x,y) - v\sigma^0_{yy}(x,y)}{E}$$

Here we have used the fact that the spatial integral of a delta function is a step function.

If we assert that an earthquake is the horizontal sliding along a fault surface, we find that we can produce a jump in shear displacement across our thin tabular box by applying a shear stress equal to

$$\sigma^0_{xz}(x,y,z) = \mu D_x(x,y)\delta(z)$$

$$\sigma^0_{yz}(x,y,z) = \mu D_y(x,y)\delta(z)$$

$$\qquad (7.10)$$

We can also produce a jump in the displacement normal to the tabular box (e.g. opening of a crack) by applying extensional stresses inside the box.

We have just described a clever method for deriving the elastic response of a medium to inelastic deformation across some surface. Instead of solving for the continuum response of that inelastic slipping region, we replace it with a region that is assumed to be linearly elastic. We introduce singular stresses on that surface (delta functions in space) that stretch the elastic surface so strongly that there is a net displacement across the stretched region. Of course, this is a physical fiction; we are using infinitesimal linear elasticity to calculate the response of infinitely large strains within the box. However, we don't really care about what is exactly happening within the box. We just want there to be an offset of one side of the box relative to the other.

If we can calculate the response of the rest of the medium to the introduction of the applied stresses in the source region, then we can calculate the response of the rest of the medium (outside the box) to a jump in the boundaries of the box. This source modeling trick is sometimes referred to as a "dislocation source." This trick of applying singular stresses to produce slip is often used in finite-element modeling. That is, forces are applied to frid points in such a way that they produce jumps in displacement. This can save effort by eliminating the need for split nodes.

It is customary to parameterize the "size" of the dislocation source by integrating the applied stress tensor $\sigma^0(x, y, z)$ over space. This integrated stress is called the **Moment tensor**; that is stress integrated over a volume has units of stress times volume, or units of force times length. These are the units of torque. That is, sources are often described by a torque (hence the origin of the word, moment). **DO NOT MISTAKE SEISMIC MOMENT FOR AN ENERGY. Although torque and energy seemingly have the same units, torque is a force and energy is … well it's energy.**

$$\mathbf{M_0} \equiv \int_0^l \int_0^w \int_0^h \sigma^0(x, y, z)\, dx\, dy\, dz \tag{7.11}$$

If the source is a simple shear dislocation across a boundary then we can substitute (7.10) into (7.11) to obtain

$$\mathbf{M_0} \equiv \int_0^l \int_0^w \int_0^h \mu \mathbf{D}(x, y)\delta(z)\, dx\, dy\, dz = \int_0^l \int_0^w \mu \mathbf{D}(x, y)\, dx\, dy \tag{7.12}$$

The size of the moment tensor is often described with the simple scalar "seismic moment," defined by

$$M_0 \equiv \mu S \overline{D} \tag{7.13}$$

where S is the rupture area and $\overline{D}$ is the average slip on the rupture surface. As we will see in a second, the seismic moment is the size scaling factor for long wavelength waves. The key elements in the scaling factor are the average slip, and the rupture area. This makes physical sense since our medium is assumed to be linear. Double the slip and we expect to double the ground motions. Also, for long wavelength waves, doubling the area should also double the ground motions.

Confusions about seismic moment

While we expect ground motions to scale linearly with rupture area and average slip, there is great confusion about the meaning of including rigidity in our size scaling factor called seismic moment. In particular, the μ is the value of rigidity inside our infinitesimally thin box. It has no real physical meaning, since we only use it to determine the size of the infinite elastic strain that is calculated using infinitesimal elasticity inside of our thin source box (a true oxymoron). Unfortunately, it has become common to hear the phrase "moment release." However, earthquakes do not release moment. When people talk about how much moment is released, what they really mean to convey is the slip D integrated over

5

the rupture area *S*. This quantity has been called **Potency** *P* by Ben Menahem and Singh (1981, *Seismic Waves and Sources*, Springer-Verlag, New York, 1108 pp) and it has units of strain integrated over a volume, which is units of volume.

$$P \equiv \int_0^l \int_0^w \int_0^h \mathbf{D}(x,y)\delta(z)dxdydz = \int_0^l \int_0^w \mathbf{D}(x,y)dxdy = S\overline{D} \tag{7.14}$$

We can also define a **Potency History** $P(t)$ as follows.

$$P(t) = \int_0^L \int_0^W D(x,y;t)dxdy \tag{7.15}$$

Point Sources

Although it is clear that earthquake sources occur primarily as slip on a surface (a fault), it is often convenient and adequate to approximate the source as having infinitesimal rupture area, but finite Potency or Seismic Moment. The solution for this problem is much simpler than that of a source with a finite rupture area. Furthermore, the point-source solution can be used as a Green's function to construct the solution to more complex sources since the medium is considered to be linear away from the fault surface.

This type of source was first introduced by Love in his classic book, A Treatise on the Mathematical Theory of Elasticity in 1927. He used the term, **nucleus of strain**, for such a point source. By that, he meant a singular strain could be introduced at a point in a medium. In order to produce finite displacements at points away from the source, it is necessary for the source to have units of volume (potency). If the material is considered to be linearly elastic, then we can also introduce a point source defined by the stress tensor at the source point, which is called the **Moment tensor**. Of course, this is even more fictitious than before since we are using infinitesimal strain theory to describe triply singular stress and strain. However, at distances large compared to the rupture lengths of a particular earthquake, and at frequencies that are low compared to times required by seismic waves to travel across the source region, a point approximation of the source is adequate for simulating earthquakes in elastic media.

It is helpful at this point to realize that the Moment tensor is simply a spatial integral of a stress tensor that is applied to the medium. Like any stress tensor, it can be decomposed into an isotropic stress $\boldsymbol{\sigma}_H$ (sometimes called hydrostatic stress) and a deviatoric stress $\boldsymbol{\sigma}'$.

$$\boldsymbol{\sigma}' = \boldsymbol{\sigma} - \boldsymbol{\sigma}_H \tag{7.16}$$

where

$$\sigma_{Hij} = \tfrac{1}{3}\sigma_{kk}\delta_{ij} \tag{7.17}$$

In stress tensors, the hydrostatic stress gives a measure of the pressure at a point and the deviatoric stress is used to describe the shearing in the medium. In a similar way, we can decompose the moment tensor into an "isotropic component"

and a deviatoric component. Now, if an earthquake is composed of unidirectional slip on a plane, then the shear strain and stress necessary to simulate that slip is very simple in the coordinate frame of the fault (see equation (7.10)). It is given by

$$\mathbf{M}_o = \begin{bmatrix} 0 & \mu S\bar{D} & 0 \\ \mu S\bar{D} & 0 & 0 \\ 0 & 0 & 0 \end{bmatrix} \tag{7.18}$$

In the principal coordinate frame, which is oriented at 45° to the fault coordinate frame, this could also be written as

$$`\mathbf{M}_o = \begin{bmatrix} \mu S\bar{D} & 0 & 0 \\ 0 & -\mu S\bar{D} & 0 \\ 0 & 0 & 0 \end{bmatrix} \tag{7.19}$$

A point source of this type is commonly called a **double-couple source**. Unfortunately, this term has also created tremendous confusion. That is, the word **non-double-couple source** is common in geophysical literature, and it is often taken to mean sources that are not well described as slip on a plane (e.g., an explosion). However, the word non-double-couple source technically means a source that is not fit with a simple shear at a point as given in (7.18) or (7.19). Earthquakes can be non-double-couple in the following ways. 1) if the earthquake has one fault plane, but the slip vector changes direction from one location to another, 2) The earthquake consists of more than one fault plane where the planes are neither parallel nor perpendicular 3) The fault is too large to be approximated as a point. In this sense, almost all earthquakes are non-double-couples. It is usually best to think clearly about what is really meant when someone tells you that the source was non-double-couple.

Reciprocity for a point force

At this point, I would like to discuss the property of reciprocity. Roughly speaking it says that the source and receiver can be interchanged for any linear continuum. Let us begin with a static deformation problem. Suppose we have a linearly elastic medium that is surrounded by a boundary that is either traction free or rigid (this is known as a **homogeneous boundary condition** and it implies that no work is done at the boundary). Now suppose that we apply point forces at two locations, $\mathbf{x}$ and ξ, as is shown in Figure 7.2. While the direction of the force is arbitrary, let us assume that the force at $\mathbf{x}$ is applied in the ith direction and that an equal amplitude force is in the j$^{\text{th}}$ direction at ξ. That is assume that

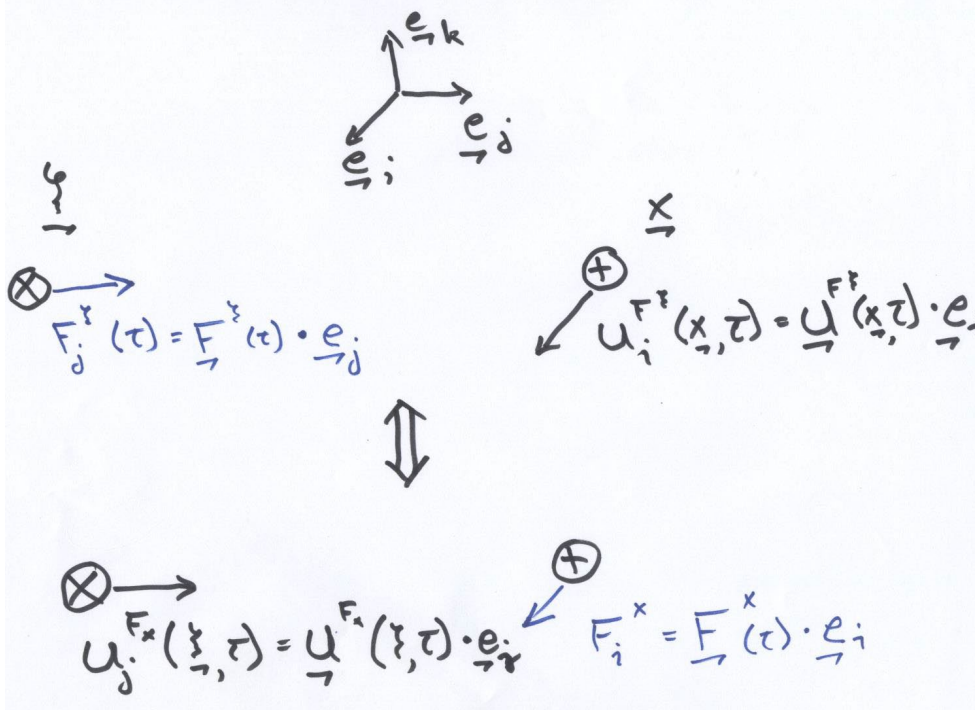$$\mathbf{F}^\xi = F\mathbf{e}_i$$
$$\mathbf{F}^x = F\mathbf{e}_j \tag{7.20}$$

Figure 7.2. The displacement time history observed in the ith direction at *x* due to a point force in the jth direction at ξ is identical to the displacement time history in the jth direction observed at ξ due to a point force in the ith direction at x. The amplitude of the two point forces are assumed to be identical. In this example i=2 and j=3.

Assume that the displacement due to the application of this force is $\mathbf{U}^{F^x}$ and $\mathbf{U}^{F^\xi}$. We first apply $\mathbf{F}^\xi$ at ξ and since the medium is linearly elastic and no work is done at the boundary, the work done by this force is just the force dotted with the displacement at ξ, or

$$W\left(F_j^\xi\right) = \frac{1}{2}\mathbf{F}^\xi \cdot \mathbf{U}^{F^\xi}$$

$$= \frac{1}{2}F_j^\xi U_j^{F^\xi}\left(\xi\right)$$

(7.21)

We now apply the second force $\mathbf{F}^x$ at $\mathbf{x}$. The work done by application of the second force is now the change in displacement $\mathbf{U}^{F^x}\left(\mathbf{x}\right)$ at $\mathbf{x}$ dotted with $\mathbf{F}^x$, but now plus the additional work done by $\mathbf{F}^\xi$ through the displacement $\mathbf{U}^{F^x}\left(\xi\right)$ at ξ. That is,

$$W\left(\mathbf{F}^\xi \text{ then } \mathbf{F}^x\right) = \frac{1}{2}\mathbf{F}^\xi \cdot \mathbf{U}^{F^\xi}\left(\xi\right) + \frac{1}{2}\mathbf{F}^x \cdot \mathbf{U}^{F^x}\left(\mathbf{x}\right) + \mathbf{F}^\xi \cdot \mathbf{U}^{F^x}\left(\xi\right)$$

$$= \frac{1}{2}\left(F_j^\xi U_j^{F^\xi}\left(\xi\right) + F_i^x U_i^{F^x}\left(\mathbf{x}\right)\right) + F_j^\xi U_j^{F^x}\left(\xi\right)$$

(7.22)

8

Now if, instead, we first applied $\mathbf{F}^x$ at $\mathbf{x}$, and then we apply $\mathbf{F}^\xi$ at ξ, then we can calculate the total work as

$$W\left(\mathbf{F}^x \text{ then } \mathbf{F}^\xi\right) = \frac{1}{2}\mathbf{F}^x \cdot \mathbf{U}^{F^x}\left(\xi\right) + \frac{1}{2}\mathbf{F}^\xi \cdot \mathbf{U}^{F^\xi}\left(\mathbf{x}\right) + \mathbf{F}^x \cdot \mathbf{U}^{F^\xi}\left(\mathbf{x}\right)$$

$$= \frac{1}{2}\left(F_j^\xi U_j^{F^\xi}\left(\xi\right) + F_i^x U_i^{F^x}\left(\mathbf{x}\right)\right) + F_i^x U_i^{F^\xi}\left(\mathbf{x}\right) \tag{7.23}$$

Now since the total energy of the system is independent of the order in which we apply the forces,

$$W\left(\mathbf{F}^x \text{ then } \mathbf{F}^\xi\right) = W\left(\mathbf{F}^\xi \text{ then } \mathbf{F}^x\right) \tag{7.24}$$

We conclude that

$$\mathbf{F}^\xi \cdot \mathbf{U}^{F^x}\left(\xi\right) = \mathbf{F}^x \cdot \mathbf{U}^{F^\xi}\left(\mathbf{x}\right)$$

$$F_j^\xi U_j^{F^x}\left(\xi\right) = F_i^x U_i^{F^\xi}\left(\mathbf{x}\right) \tag{7.25}$$

Now since the forces at the two sites are equal in amplitude, this means that the displacements at the two sites must also be equal in amplitude. That is, the displacement in the ith direction at $\mathbf{x}$ due to a force in the jth direction at ξ is the same as the displacement in the jth direction at ξ due to a force in the ith direction at $\mathbf{x}$. This can be generalized to the dynamic displacements that occur in a linear medium. For derivations see Chapter 2 of Aki and Richards (Quantitative Seismology, second edition) or see section 15.6 of Fung (Foundations of Solid Mechanics).

Now if we write the displacements using Green's functions $G_{ij}\left(\mathbf{x},t;\xi\right)$ for a point force in the jth direction at ξ that produces a displacement time history in the ith direction at $\mathbf{x}$.

$$U_i^{F^\xi}\left(\mathbf{x},t\right) = G_{ij}\left(\mathbf{x},t;\xi\right) * F_j^\xi\left(t\right) \tag{7.26}$$

No summation convention! If we switch the locations of the source and observer, but we now assume that the point force is in the ith direction (the direction of the observed ground motion at x) and that the observed motion at ξ is in the jth direction (the direction of the applied force at ξ) we obtain

$$U_j^{F^x}\left(\xi,t\right) = G_{ji}\left(\xi,t;\mathbf{x}\right) * F_i^x\left(t\right) \tag{7.27}$$

Since the system is linear, the virtual work obtained by the product of the force and the displacement must be the same if the same amplitude force is applied along the displacement at the source and observer points. That is, similar to the static case, but now the work is the integral over time

$$\int_{-\infty}^{\infty} F_j^\xi\left(t\right) U_j^{F^x}\left(\xi,t\right) dt = \int_{-\infty}^{\infty} F_i^x\left(t\right) U_i^{F^\xi}\left(\mathbf{x},t\right) dt \tag{7.28}$$

Where

$$F_j^\xi\left(t\right) = F_i^x\left(t\right) \tag{7.29}$$

Since (7.28) is true for any time history for the force, it must be true that

$$U_j^{F^x}\left(\xi,t\right) = U_i^{F^\xi}\left(\mathbf{x},t\right) \tag{7.30}$$

9

Substituting (7.26) and (7.27) into(7.30), we get

$$G_{ji}\left(\xi,t;\mathbf{x}\right)*F_i^x\left(t\right)=G_{ij}\left(\mathbf{x},t;\xi\right)*F_j^\xi\left(t\right) \tag{7.31}$$

From which we can conclude that

$$G_{ji}\left(\xi,t;\mathbf{x}\right)=G_{ij}\left(\mathbf{x},t;\xi\right) \tag{7.32}$$

This is the usual statement of reciprocity. If we substitute (7.32) into (7.27), we get

$$U_j\left(\xi,t;\mathbf{x}\right)=G_{ij}\left(\mathbf{x},t;\xi\right)*F_i^x\left(t\right) \tag{7.33}$$

Reciprocity for force couples

Suppose that we consider the displacement at x caused by a force couple (see figure 7.3).
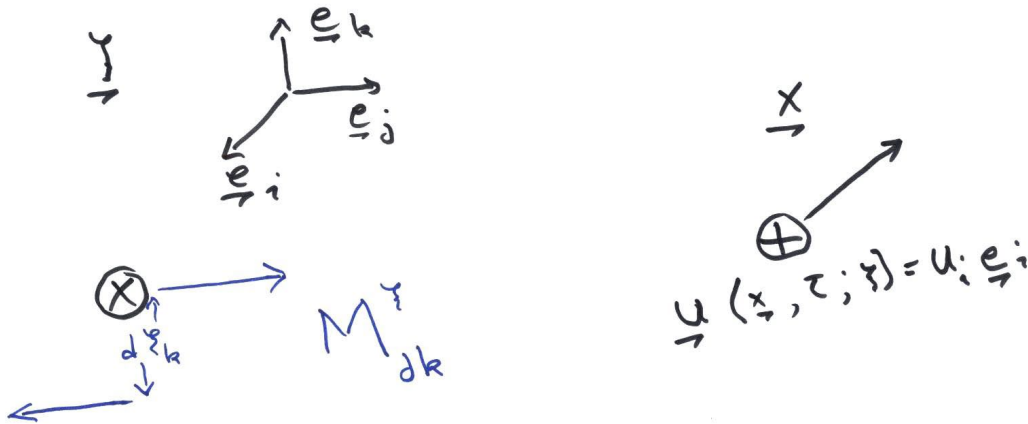
Figure 7.3. Displacement observed at x due to a force couple at ξ.
Specification of the orientation of the force couple requires two vectors, the direction of the force and the direction of the moment arm.

Now if the source is a force couple, $M_{jk}^\xi\left(t\right)\equiv\dfrac{\partial F_j^\xi\left(t\right)}{\partial\xi_k}$, and if our observer is

measuring displacement at x, then

$$U_i^{M^\xi}\left(\mathbf{x},t\right)=M_{jk}^\xi*\frac{\partial G_{ij}\left(\mathbf{x},t;\xi\right)}{\partial x_k} \tag{7.34}$$

In this case, we cannot exchange the source and the receiver. To begin with, one cannot derive the virtual work done by a torque operating on a displacement. In addition, the orientation of the force couple requires two vectors, the orientation of the force and the orientation of the gradient. However, the displacement only describes one orientation. In the case of force couples, reciprocity must be stated in terms of displacement gradients as shown in Figure 7.4.
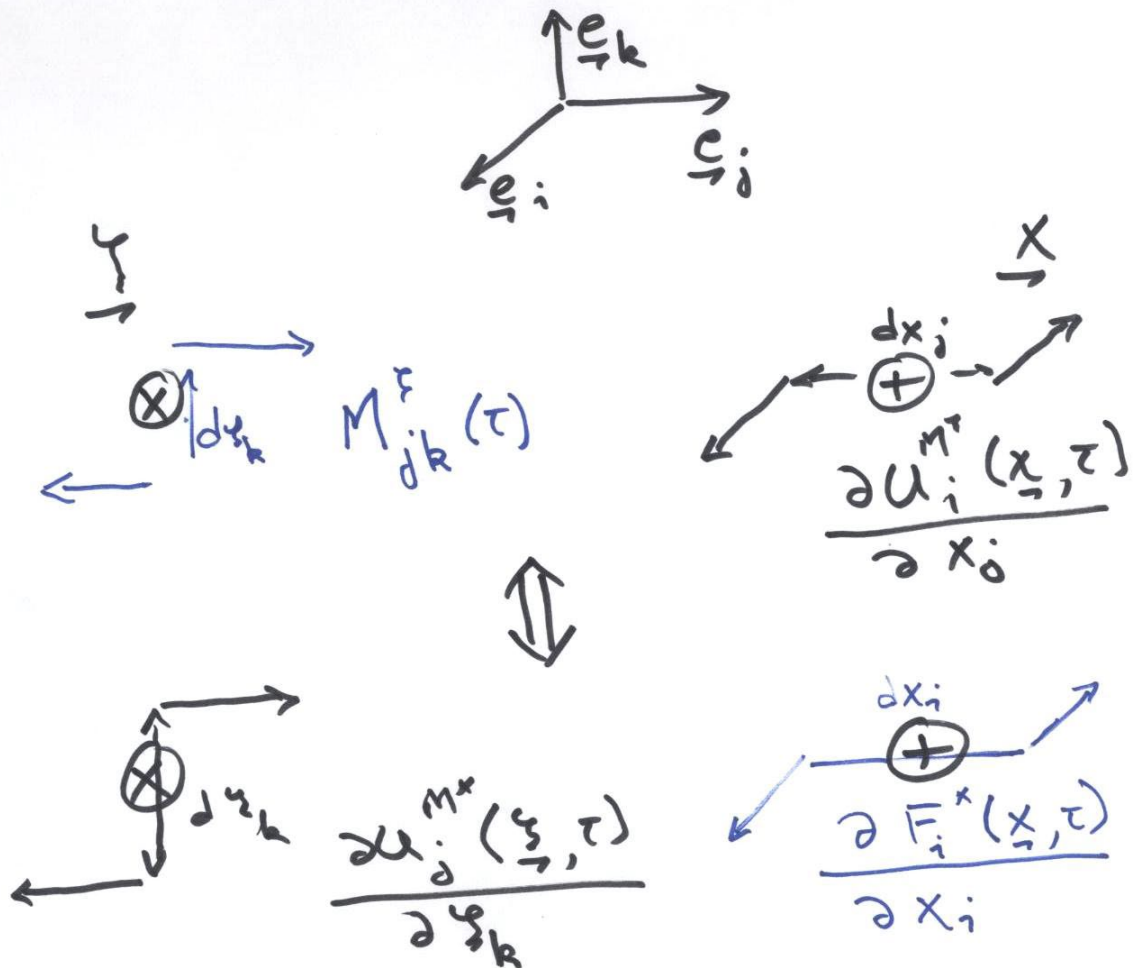
Figure 7.4. Reciprocity for a force couple at ξ involves observing a displacement gradient at x. The resulting time history of the displacement gradient is the same as the time history of a displacement gradient observed at ξ, but with the force couple at x, and with the orientation of the observation of the displacement gradient.

In this case the principle of virtual work is stated in terms of a torque times a rotation (similar to strain energies) at the source and receiver. That is,

$$\int_{-\infty}^{\infty} M_{jk}^{\xi}(t) \frac{\partial U_j^{M^x}(\xi,t)}{\partial \xi_k} dt = \int_{-\infty}^{\infty} \frac{\partial U_i^{M^\xi}(\mathbf{x},t)}{\partial x_l} M_{il}^x(t) dt \tag{7.35}$$

Where $M_{jk}^{\xi}(t) = M_{lm}^x(t)$, and as before this implies that

$$\frac{\partial U_j^{M^x}(\xi,t)}{\partial \xi_k} = \frac{\partial U_i^{M^\xi}(\mathbf{x},t)}{\partial x_l} \tag{7.36}$$

where

$$U_i^{M^\xi}(\mathbf{x},t) = \frac{\partial G_{ij}(\mathbf{x},t;\xi)}{\partial \xi_k} * M_{jk}^{\xi}(t) \tag{7.37}$$

11

And

$$U_j^{M^x}(\xi,t) = \frac{\partial G_{ji}(\xi,t;\mathbf{x})}{\partial x_l} * M_{il}^x(t)$$ (7.38)

Substituting (7.37) and (7.38) into (7.36) we obtain

$$\frac{\partial^2 G_{ji}(\xi,t;\mathbf{x})}{\partial \xi_k \partial x_l} * M_{il}^x(t) = M_{jk}^\xi(t) * \frac{\partial^2 G_{ij}(\mathbf{x},t;\xi)}{\partial x_l \partial \xi_k}$$ (7.39)

Since the moment time histories are all assume to be the same, reciprocity for force couples can be written as

$$\frac{\partial^2 G_{ji}(\xi,t;\mathbf{x})}{\partial \xi_k \partial x_l} = \frac{\partial^2 G_{ij}(\mathbf{x},t;\xi)}{\partial x_l \partial \xi_k}$$ (7.40)

This same result could have been obtained from the force statement of reciprocity. That is, if we differentiate (7.32) with respect to the kth direction at the point the force is applied, then

$$\frac{\partial G_{ij}(\mathbf{x},t;\xi)}{\partial \xi_k} = \frac{\partial G_{ji}(\xi,t;\mathbf{x})}{\partial x_k}$$ (7.41)

Similarly, if we differentiate (7.41) with respect to the lth direction at the point of observation, we obtain

$$\frac{\partial^2 G_{ij}(\mathbf{x},t;\xi)}{\partial x_l \partial \xi_k} = \frac{\partial^2 G_{ji}(\xi,t;\mathbf{x})}{\partial \xi_l \partial x_k}$$ (7.42)

Which is identical to the result obtained in (7.40). Fung shows that this result also applies to any linear visco-elastic material.

Point Double-Couple in an isotropic Whole Space

Consider a point double-couple source whose orientation is shown in Figure 7.5. Since we are using a point source in a homogeneous space, we expect to see radially spreading waves and we use spherical coordinates (r,ϕ,ζ) to describe the location of the observer. However, it is customary to describe the orientation of the fault with respect to a local coordinate system that is North, East, and up.

To describe the orientation of the rupture, we use Euler angles, and proceed in the following way. 1) Determine the **dip** angle δ of the fault. This is always between 0° (a flat plane) and 90° (a vertical plane). 2) Determine the **strike** angle θ of the fault. This is between 0° and 360° and it is the angle between geographic North and the surface projection of the fault plane. A 0° strike designates a fault that dips to the East, a 90° strike dips to the South, a 180° strike dips to the West, and a 270° strike dips to the North. 3) Determine the **rake** angle of the slip on the fault plane. A rake angle of 0° signifies a left-lateral slip (usually called **left-**

lateral strike-slip), in which case the opposite side of the fault moves horizontally and to the left when looking across the fault. A rake of 90° signifies that the "**hanging wall**" moves vertically upward over the "**foot wall**," which is usually referred to as thrust type of motion and which produces crustal shortening. Hanging wall and foot wall are mining terms used for dipping seams of coal. When walking down the dipping surface of the mine, the hanging wall is the overhead surface (the ceiling), and the footwall is the floor. A rake of 180° signifies right-lateral strike-slip motion. A rake of 270° means the hanging wall moves downward with respect to the footwall. This is usually referred to as a **normal** fault and it results in stretching of the Earth's crust.
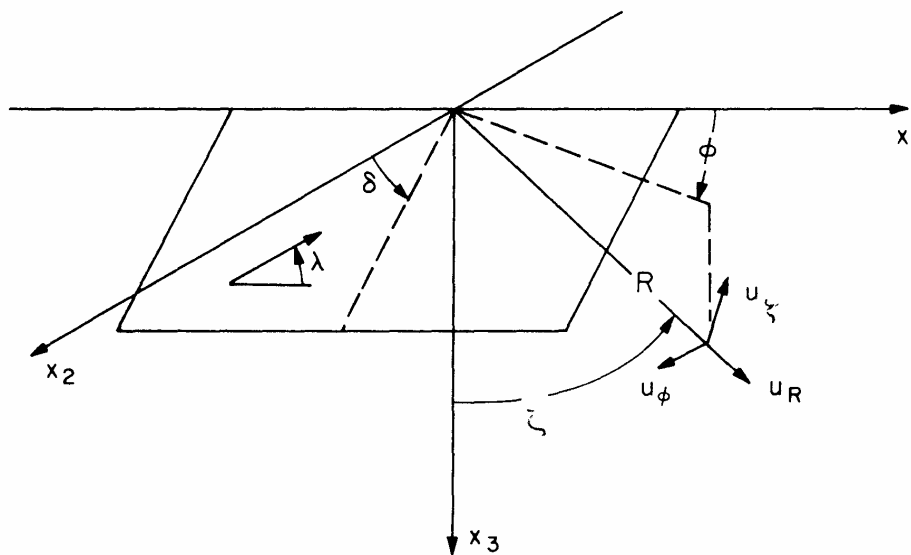

Figure 7.5. Shows the spherical coordinate system used together with the angles that describe the orientation of the fault and slip vector.

While the strike angle θ is defined with respect to geographic north, the observer's azimuth ϕ in Figure 7.2 is defined with respect to the strike line of the fault plane. We assume that the motion on a fault of area S (a very small area) is given by

$$D(t) = D\,\mathrm{H}(t) = \begin{cases} 0 & t < 0 \\ D & t > 0 \end{cases} \qquad (7.43)$$

In this case the solution can be found by differentiating the point source solution (Equation 3.85) with respect to the appropriate source coordinate (this gives us a shear-couple of forces). This solution is then summed with the solution for a perpendicular force couple which gives a double-couple solution. The solution for displacement is

13

$$G_R = \frac{S\bar{D}\Re_R(\theta,\delta,\lambda,\phi,\zeta)}{4\pi} \begin{cases} 0 & ;t < \frac{r}{\alpha} \\[2mm] \frac{\beta^2}{\alpha^2}\left[\frac{\delta\left(t-\frac{r}{\alpha}\right)}{\alpha r} - \frac{1}{2r^2} + \frac{9\alpha^2 t^2}{2r^4}\right] & ;\frac{r}{\alpha} < t < \frac{r}{\beta} \\[2mm] \frac{(3\alpha^2 - \beta^2)}{2\alpha^2 r^2} & ;t > \frac{r}{\beta} \end{cases}$$

(7.44)

and

$$G_\xi = \frac{S\bar{D}\Re_\xi(\theta,\delta,\lambda,\phi,\zeta)}{4\pi} \begin{cases} 0 & ;t < \frac{r}{\alpha} \\[2mm] \frac{\beta^2}{\alpha^2}\left[\frac{1}{r^2} + \frac{3\alpha^2 t^2}{r^4}\right] & ;\frac{r}{\alpha} < t < \frac{r}{\beta} \\[2mm] \frac{\delta\left(t-\frac{r}{\beta}\right)}{\beta r} + \frac{\beta^2}{\alpha^2 r^2} & ;t > \frac{r}{\beta} \end{cases}$$

(7.45)

Where ξ signifies either the ϕ or the ζ direction . The notation G_R and G_ξ are used to signify that this is the Green's function for a point dislocation in a whole space, and they signify displacements in the corresponding directions. Notice that everything is linearly scaled by $S\bar{D}$, which is the Potency. It is common to write this solution using the Seismic Moment M_O, but these expressions always end up being written as $\frac{M_O}{\mu}$.

I apologize for the complication that λ is used to signify both the first Lame constant and also the rake angle. The factors $\Re_R(\theta,\delta,\lambda,\phi,\zeta)$ and $\Re_\xi(\theta,\delta,\lambda,\phi,\zeta)$ signify the **Radiation pattern** and they are given by

$$\Re_R(\theta,\delta,\lambda,\phi,\zeta) = \cos\lambda\left(\sin\delta\sin^2\zeta\sin 2\phi - \cos\delta\sin 2\zeta\cos\phi\right)$$
$$+ \sin\lambda\left[\sin 2\delta\left(\cos^2\zeta - \sin^2\zeta\sin^2\phi\right) + \cos 2\delta\sin 2\zeta\sin\phi\right]$$

(7.46)

$$\Re_\zeta(\theta,\delta,\lambda,\phi,\zeta) = \cos\lambda\left(\tfrac{1}{2}\sin\delta\sin 2\zeta\sin 2\phi - \cos\delta\cos 2\zeta\cos\phi\right)$$
$$- \sin\lambda\left[\tfrac{1}{2}\sin 2\delta\sin 2\zeta\left(1+\sin^2\phi\right) - \cos 2\delta\cos 2\zeta\sin\phi\right]$$

(7.47)

$$\mathfrak{R}_\phi\left(\theta,\delta,\lambda,\phi,\zeta\right) = \cos\lambda\left(\sin\delta\sin\zeta\cos2\phi+\cos\delta\cos\zeta\sin\phi\right)$$
$$+\sin\lambda\left(\cos2\delta\cos\zeta\cos\zeta-\tfrac{1}{2}\sin2\delta\sin\zeta\sin2\phi\right) \tag{7.48}$$

Since the problem is linear, we can find the solution for any potency rate history by convolving solutions (7.44) and (7.45) with any potency rate function $\dot{P}(t) \equiv \partial(SD)\big/\partial t$.

While this solution may look complex, it is the simplest solution that approximates an earthquake and it is important to gain some physical intuition about the different parts of this solution. Let's start with the radial displacements given by equation (7.44). In Figure 7.6, I sketch the nature of the solution at several different distances. Notice that there is an impulse function in the radial component that arrives at the P-wave time, and its amplitude decays with distance as $\frac{1}{r}$. This is the **far-field P-wave** and its time history is the time derivative of the Potency on the fault. Its amplitude is also scaled by the inverse of the P-wave velocity α. That is, the far-field waves are the transient part of the solution, and they carry the **radiated energy** in the wavefield. These radiated waves become smaller as the stiffness of the medium increases or as the density decreases. The amplitude of the far-field P-wave is different at different take-off angles and this amplitude is determined by $\mathfrak{R}_R$. Since the power flux through a surface depends on surface integral of $\dot{u}^2 \sim \frac{1}{r^2}$, the *power flux of far-field waves through any sphere centered on the source is independent of the radius sphere*. Hence, in the absence of anelastic attenuation, the energy of the radiated wave is constant in time.

Now notice that after the arrival of the far-field P-wave, there is a term that is constant in time up until the S-wave arrives. This term is part of **the near-field P-wave** and its amplitude decays with distance as $\frac{1}{r^2}$. There is also a second near-field term that begins after the P-wave arrives. It grows in time as t^2 and decays with distance as $\frac{1}{r^4}$. While this tern may look like a very near-field term, notice that by the time of the S-wave, its amplitude has grown to order
$$\left(t_S-t_P\right)^2 = r^2\left(\frac{1}{\beta}-\frac{1}{\alpha}\right),$$
so it is actually of the same order as the other near-field terms. This very-near-field term (which behaves like the second time integral of the Potency time history) only exists up until the time of the S-wave arrival. After the S-wave arrival, the radial displacement is simply a constant in time; this is the static offset and it decays in distance as $\frac{1}{r^2}$.

The tangential components of the motion (equation (7.45)) are also of interest. Notice that there is a near-field P-wave static term that starts at the P-wave arrival

15

time (yes there truly are P-waves on the tangential component). This is also accompanied by a very-near-field term that exists only between the P- and S-wave arrival times. The far-field S-wave then arrives and the solution then becomes the static displacement in the tangential directions. **Notice that the far-field S-wave is larger than the far-field P-wave by a ratio** of α^3/β^3 (this is a factor of 5.2 for a Poisson solid). Figure 7.3 shows the nature of the solution at different distances.
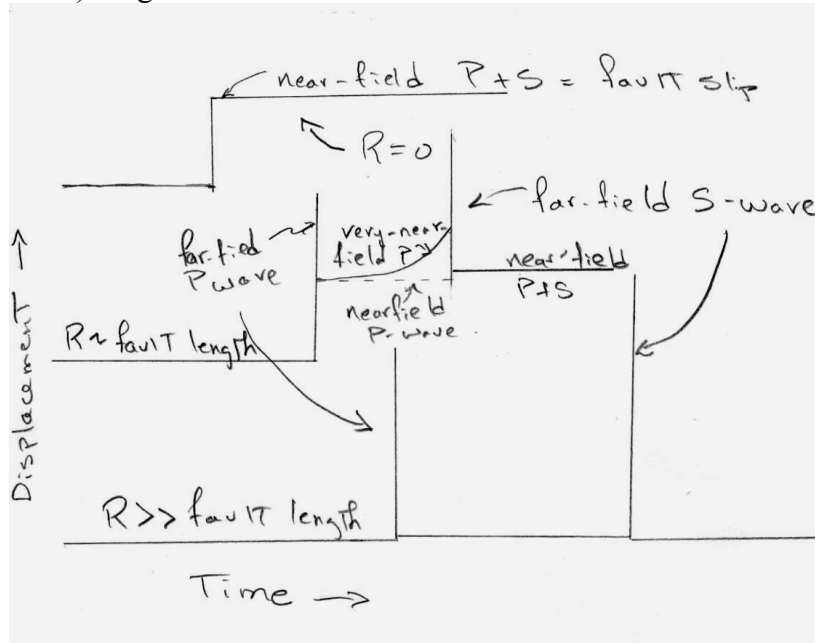
Figure 7.6 Cartoon showing the characteristics of the displacements generated by a point double couple source in a whole space. Far-field P- and S-waves have a time history that is the first time derivative of the potency time history and they decay as $1/r$. Near-field terms have the same time behavior as the potency history and they decay as $1/r^2$. Very-near-field terms only occur between the P- and S- arrival times, they have a time behavior that is the 2nd time integral of potency, and they decay as $1/r^4$.

Radiated energy from a point source

Normally, we consider the radiated energy to be the part of the energy that is associated with the waves long after the earthquake is over (assuming that there is no anelastic attenuation). In this case, we consider only the far-field terms and the radiated energy is the integral over time of power $p(r,t)$ through an enclosing surface at large distance r. That is,

$$E_R \sim r^2 \int_{starttime}^{endtime} p(r,t)\,dt \qquad (7.49)$$

16

The power through any point on the surface is particle velocity times the stress associated with the traveling wave, or

$$p(r,t) = \dot{u}(r,t)\sigma(r,t) \tag{7.50}$$

In a traveling far-field S-wave (which contains most of the radiated energy), the stress scales as

$$\sigma \sim \rho\beta\dot{u} \sim \rho\beta\ddot{P}(t)\Big/\beta r = \rho\ddot{P}(t)\Big/r \tag{7.51}$$

Therefore, the power scales as

$$p(r,t) \sim \rho\beta\dot{u}^2 \sim \rho\beta\left(\ddot{P}(t)\Big/\beta r\right)^2 = \rho\ddot{P}^2(t)\Big/\beta r^2 \tag{7.52}$$

Therefore, the radiated energy scales as

$$E_R \sim \rho \int_{starttime}^{endtime} \ddot{P}^2(t)\Big/\beta\, dt \tag{7.53}$$

This interesting result says that the radiated energy scales as the **2nd time derivative of the Potency history**. That is, *there is no radiated energy when the source is rupturing at a steady rate.*

Radiation Pattern

In addition to the time behavior and distance decay, there are a number of geometric factors $\left(\Re_r, \Re_\phi, \Re_\varsigma\right)$ given by equations (7.46) to (7.48) that determine the amplitude and direction of the particle motions of the solution. These factors are particularly important to engineering seismology, since they determine where the S-wave is going to be large. Unfortunately, these factors are complex enough that it is very hard to gain intuition simply by looking at equations (7.46) to (7.48). I like to use a simple tool to remind myself of the radiation pattern. This tool is called a **focal sphere** and an example of one is shown in Figure 7.7. I strongly suggest that you construct one for yourself (a softball and a magic marker work well), and that you learn how to use it.

Figure 7.7. A Focal Sphere. This is an idealization of the far-field
waves from a point shear at the center of the sphere. The two planes that
cut the sphere are the conjugate fault planes and the sense of slip on
these two planes are shown by the arrows at the intersection of the
planes.

The surface of the sphere represents an outgoing far-field wavefront (either a P- or
an S-wave) from a point double couple. The sphere is cut by two perpendicular
planes that represent the two conjugate slip planes. While real earthquakes occur
on only one of these planes, when the source is approximated by a point double-
couple, then the two conjugate planes produce identical deformations everywhere
in the medium. Remember that the source is basically a point shear strain and that
both stress and strain are symmetric tensors.

Notice that the conjugate slip planes divide the sphere into four quadrants, two of
which are light colored and two are dark. This pattern is commonly referred to as
a **beach ball** and seismologists commonly use it to show the orientation of the
earthquake rupture (the strike, dip, and rake). The dark quadrants are used to show
locations on the focal sphere where the P-wave is compressional (or radially
outward from the source) and the light quadrants show where the P-wave is
dilational (or radially inward towards the source). While there are some
exceptions, it is traditional to display the lower hemisphere of the focal sphere as it
would be projected on a horizontal plane and viewed from directly above the
source.

The far-field S-wave radiation pattern is denoted by the arrows on the focal sphere.
That is, the arrows give the directions of the particle motion for the far-field S-
waves. The points of intersection of the two planes turn out to be nodes for all

18

motions (far-field P- S-, near-field motions, everything). These "super nodes" turn out to be 1) directly above a vertical strike slip rupture, 2) directly along strike for a dipping thrust or normal fault. At 90º from these super-nodal points, and along both fault planes, the far-field S-wave attains its maximum value. Somewhat surprisingly, the direction of this maximum far-field S-wave is perpendicular to the fault plane. **I could draw many sketches trying to show what this radiation pattern looks like, but it is really better for you to make yourself a focal sphere and learn how to use it.**

Figure 7.8 shows some very interesting accelerograms recorded on SMA-1's for a M4.9 earthquake in the Imperial Valley, CA. The Imperial Valley is a deep basin filled with the sediments of the Colorado River delta. Seismic velocities in this basin increase continuously with depth; the overburden pressure compacts the sediments. This velocity gradient means that seismic rays are nearly vertically incident near the Earth's surface. Hence the P-waves are exclusively observed on the vertical component of the motion and the S-waves are observed on the horizontal components. Well, that is except for near-field P-waves that can be seen as the long-period ramp that precedes the S-wave arrival on several of the horizontal records. Notice that the far-field P-waves are much higher frequency than the S-waves. This is surprising since equations (7.44) and (7.45) indicate that the P- and S-wave Green's functions have the same behavior for the far-field waves; that is, they are both delta functions for a step function in potency. As it turns out, if the P-waves in these records are low-pass filtered then they do look similar to the S-waves (except that they are smaller, as they ought to be). So one explanation for this difference in frequency content of the P- and the S-waves is that both start the same at near the earthquake, but by the time they get to Earth's surface stronger anelastic attenuation of the S-wave causes the S-wave to be more attenuated than the P-wave. In Chapter 8, I suggest an alternative explanation; perhaps there are high-frequency dilatations happening on the rupture surface (acoustic fluidization).

While differences in anelastic wave attenuation may help to explain the different frequency contents of P- and S-waves, there is more to this problem. Figure 7.9 shows a polar plot of the amplitude of the far-field waves. That is the amplitude of the far-field waves are first corrected to be at the same distance, and then their amplitude is plotted as the radial distance from the origin for the appropriate direction to the observer. The expected amplitudes are the clover leaf pattern. What we see is that the amplitude of the low-pass filtered motion behaves as it should (according to our solution). However, the high-frequency waves do not have any apparent correlation with the expected radiation pattern. It is my experience that radiation pattern is clearly observable when the frequency is approximately $1 \big/ (\text{duration of the earthquake})$ but that radiation pattern is generally not observable for frequencies higher than $10 \big/ (\text{duration of the earthquake})$.

While there are several speculations about why the radiation pattern "disappears" at high frequencies, I am not aware of a compelling study that explains this observation. Some have suggested that the breakdown in radiation pattern is due to short scale complexity in the source's geometry (a non-planar fault), others have suggested that there may be something happening other than pure shear sliding (dilatation?), and others have suggested that it has nothing to do with the source, but is caused by scattered waves. We will come back to these high-frequency waves in Chapter 8. At this point though, I think that it is sufficient to say that low-frequency waves can be explained by shear faulting on a plane in an elastic medium. High-frequency waves are usually best modeled as sources of random noise without any systematic azimuthal variation in amplitudes.

448   THE IMPERIAL VALLEY, CALIFORNIA, EARTHQUAKE OF OCTOBER 15, 1979

FIGURE 298.—Original accelerograms from M_L=4.9 aftershock of October 16, 1979. Records are shown from north (top) to south (bottom) in order of increasing epicentral distance. Time trace at tip of each record gives a code with 5 (downward) pulses per second; code is interpreted as in Kinemetrics, Inc. (1977). Clock corrections at time of aftershock are also shown. Numbers to right on each trace indicate longitudinal, vertical, and transverse azimuths from top to bottom, respectively. A, Northern four records. B, Southern four records.
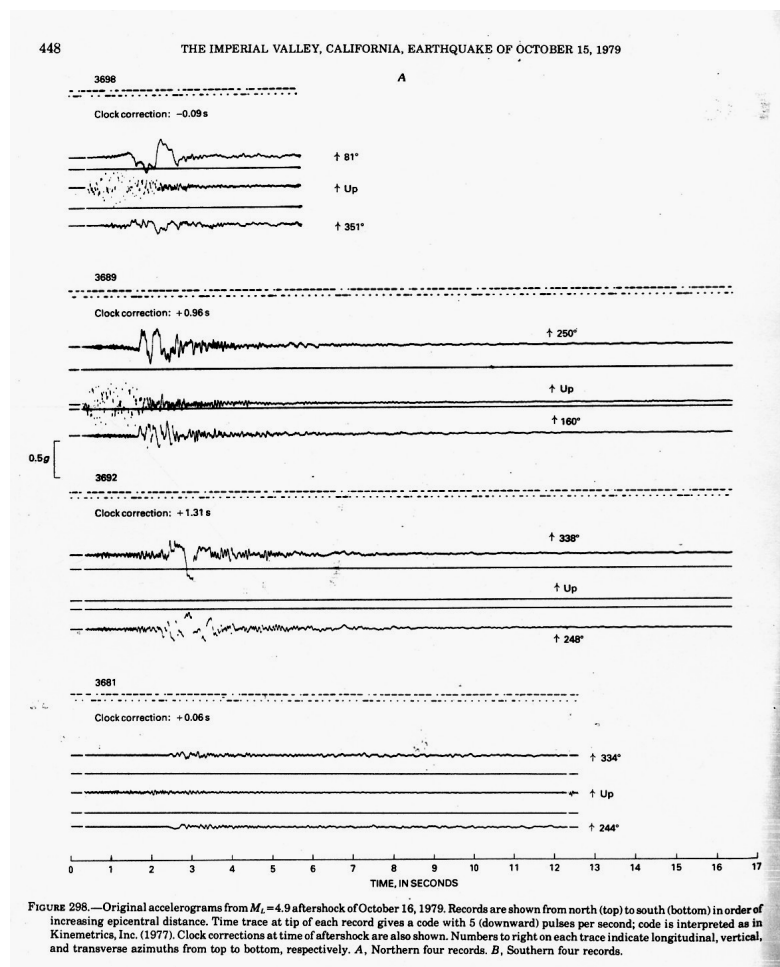
Figure 7.8. These are four near-source accelerograms recorded from a M 4.9 earthquake in the Imperial Valley, which is a large basin with deep horizontally layered sediments. Notice that the P-wave, which is observed on the vertical components, is much higher in frequency than the S-wave, which is seen on the horizontal components. Also notice the very-near-field waves seen on the horizontal accelerations before the S-wave arrives.
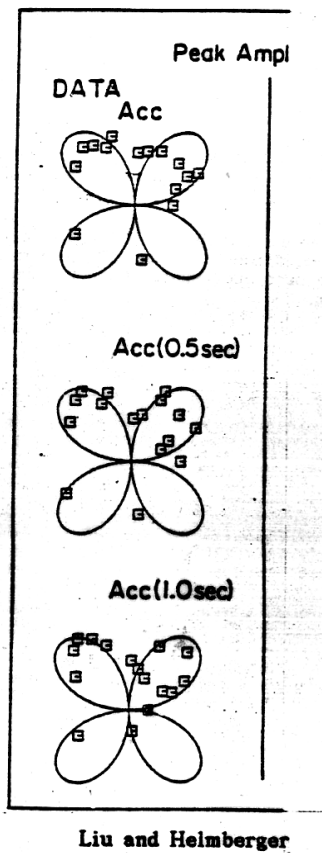
20

Liu and Helmberger

Figure 7.9. Polar plot of P-wave amplitudes (radial distance is amplitude at different azimuths) for a vertical strike slip earthquake in the Imperial Valley. The amplitudes are all corrected to the same distance and the "clover-leaf" pattern is the expected amplitude variation of far-field P-waves as a function of station azimuth. The raw acceleration records are dominated by high-frequency motions (> 5 Hz) and they show no apparent systematic variation with azimuth. However, when the records are low-pass filtered at 1 Hz, then there is a reasonable correspondence between the observed and predicted amplitudes.

Finite Sources
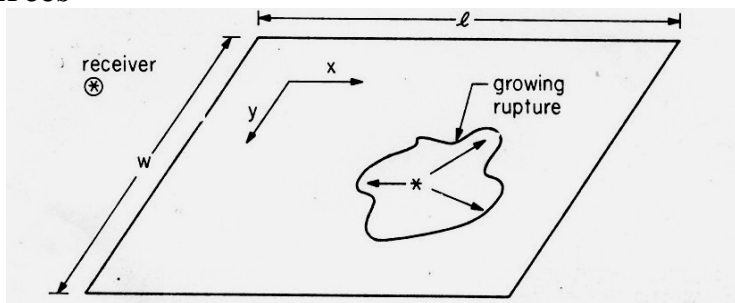
Figure 7.10. Simplified geometry of a finite fault model.

Of course, there are no true point sources in nature. Point sources can be useful approximations when the observer is at large distances compared with the source dimension and when the period of interest is long compared to wave travel times across the source region. However, it turns out that for many interesting problems, this approximation is not valid. While general seismic sources may involve inelastic deformations within a volume, it seems that many earthquakes can be simulated as slip on a plane. In this case we can write the solution at a point **X** (bold capital x is the vector location of the observer) by integrating the Green's function over the rupture surface. That is,

$$\mathbf{u}(\mathbf{X},t) = \int_0^L \int_0^W \dot{\mathbf{D}}(x,y,t) * \mathbf{G}(x,y;\mathbf{X};t)\, dy\, dx \tag{7.54}$$

Where x and y are coordinates on the rupture surface, and $\mathbf{G}(x,y;\mathbf{X};t)$ is the vector Green's function for a point dislocation (a vector in the x,y plane) at (x,y) as observed at **X**. The * operator signifies a kind of generalized convolution in which each of the components of **D** and **G** are convolved. Since the source is finite, it is no longer convenient to choose spherical coordinates. In fact, since the source is located on a plane, it may be convenient to choose Cartesian coordinates. However, it is important to realize that the expression for the Green's function may become a very complex expression. Of course, it is a fairly straightforward procedure to solve (7.54) numerically once we know what **G** looks like, which is a difficult problem. However, if we are interested in the characteristics of the far-field waves, then we can approximate the Green's function as a sum of rays. Each ray represents either a P- or S-wave that travels to the receiver by a combination of refractions and reflections off of layer boundaries (see Chapter 4). That is, we can approximate the Green's function as

$$\mathbf{G}(x,y,t) = \sum_{i=1}^{\infty} \mathbf{G}_i(x,y,t) \tag{7.55}$$

Where we have dropped the coordinate of the fixed receiver, **X**, for convenience. For the case of a homogeneous space, there are only two rays to consider, direct P and Direct S. In the case of a homogeneous half-space, there are 6 rays to consider P, pP, sP, S, pS, and sS. The pP is a ray that travels upward from the source as a P-wave and is then converted into an SV-wave when it reflects off of the free surface. Likewise, sP leaves the source as an S-wave and then is converted into a P-wave when it reflects off the free surface. When the medium has more complexity than a half-space (e.g., a layer over a half space) then there are an infinite number of possible rays, although many of them are very small since they involve multiple reflections, each of which may involve a significant loss of energy.

If we are observing the source at a distance, then make the following approximation.

$$\mathbf{G}_i(x,y,t) \approx \mathbf{G}_i\left[x_0, y_0, t - T_i(x,y)\right] \tag{7.56}$$

22

Where (x_0, y_0) is some point on the fault plane (arbitrarily choose one), and $T_i(x, y)$ is the difference in the ith ray's arrival times for two point sources located at (x, y) and (x_0, y_0). We can rewrite (7.56) as

$$\mathbf{G}_i(x, y, t) \approx \mathbf{G}_i(x_0, y_0, t) * \delta\left[t - T_i(x, y)\right] \tag{7.57}$$

Where δ is a Dirac delta function. Substituting (7.56) into (7.55) into (7.54), we obtain

$$\mathbf{u}(t) \approx \int_0^L \int_0^W \sum_{i=1}^{\infty} \mathbf{G}_i(x_0, y_0, t) * \delta\left[t - T_i(x, y)\right] * \dot{\mathbf{D}}(x, y, t) \, dy \, dx$$

$$= \sum_{i=1}^{\infty} \mathbf{G}_i(x_0, y_0, t) * \int_0^L \int_0^W \dot{\mathbf{D}}\left[x, y, t - T_i(x, y)\right] dy \, dx \tag{7.58}$$

$$= \sum_{i=1}^{\infty} \mathbf{G}_i(x_0, y_0, t) * \mathbf{F}_i(t)$$

Where

$$\mathbf{F}_i(t) \equiv \int_0^L \int_0^W \dot{\mathbf{D}}\left[x, y, t - T_i(x, y)\right] dy \, dx \tag{7.59}$$

$\mathbf{F}_i(t)$ is called the **far-field time function** for the ith ray, and it is a function of time that is controlled by the spatial and temporal pattern of slip on the rupture surface. If we ignore the travel time difference in (7.59), then we obtain the **moment rate function,** which is defined as

$$\dot{M}_0(t) \equiv \mu \int_0^L \int_0^W \dot{D}(x, y, t) \, dy \, dx \tag{7.60}$$

In (7.59) we kept track of the fact that slip is a vector quantity whose orientation (rake angle) can change with position on the fault. It is customary to define the moment rate function as a scalar quantity that depends on the integral of the amplitude of the slip vector over the rupture surface.

If the seismogram at a station is dominated by a particular ray (for instance the teleseismic P-wave from a deep earthquake), then the ground displacement at a station is largely determined by the far-field time function and anelastic attenuation that occurs during wave propagation. As an example, consider a simple Earth model in which P- and S-waves travel through a homogeneous half-space. Of course, the actual Earth is a spheroid with a complex structure. However, when P- or S-waves are observed at distances between 30° to 90° from the source, they appear to propagate without dispersion and the Green's functions for the P- and S-wave portions of the seismogram can be written as

$$\mathbf{G}_P(x,y) \approx \left\{ A_p \delta\left[t - T_P(x,y)\right] + A_{pP} \delta\left[t - T_{pP}(x,y)\right] + A_{sP} \delta\left[t - T_{sP}(x,y)\right] \right\} \mathbf{e}_P * Q_P(t)$$

(7.61)

$$\mathbf{G}_S(x,y) \approx \left\{ A_s \delta\left[t - T_S(x,y)\right] + A_{pS} \delta\left[t - T_{pS}(x,y)\right] + A_{sS} \delta\left[t - T_{sS}(x,y)\right] \right\} \mathbf{e}_S * Q_S(t)$$

(7.62)

Where the phases *P, pP, sP,* etc. are shown in Figure 7.9. $\mathbf{e}_p$ and $\mathbf{e}_S$ are unit vectors in the direction of the P- and S-wave particle motions at the receiver. A_P, A_{pP}, A_{sP}, etc. are amplitude factors that depend on the distance of the source (geometric spreading of the wavefront) and on the radiation pattern for the ray as it leaves the source [see equations (7.44) through (7.48)]. Finally $Q_P(t)$ and $Q_S(t)$ are Q operators for the P- and S-waves, respectively. That is, they are a kind of low-pass filter. Substituting (7.61) and (7.62) into (7.58), we find that the teleseismic P- and S-waves are approximately given by

$$\mathbf{u}_P(x,y) \approx \left\{ A_p F_P\left[t - T_P(x_0,y_0)\right] + A_{pP} F_{pP}\left[t - T_{pP}(x_0,y_0)\right] + A_{sP} F_{sP}\left[t - T_{sP}(x_0,y_0)\right] \right\} \mathbf{e}_P * Q_P(t)$$

(7.63)

$$\mathbf{u}_S(x,y) \approx \left\{ A_s F_S\left[t - T_S(x_0,y_0)\right] + A_{pS} F_{pS}\left[t - T_{pS}(x_0,y_0)\right] + A_{sS} F_{sS}\left[t - T_{sS}(x_0,y_0)\right] \right\} \mathbf{e}_S * Q_S(t)$$
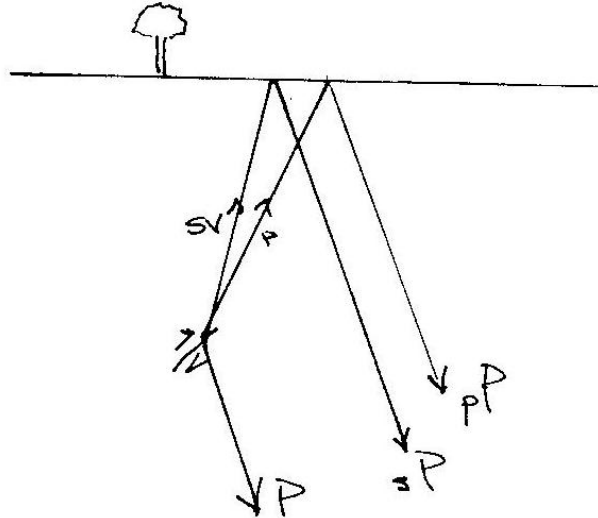
(7.64)

Figure 7.11 Idealization of the rays that comprise the P-wave group observed at teleseismic distances.

I show some examples in Figure 7.12 of how teleseismic P-waves are generated from (7.63). I assume a vertical strike-slip fault with a circular rupture whose diameter is 12 km and whose center is located at a depth of 7 km. The observer is located at a distance of 58º directly along the strike. The rupture velocity is assumed to be 2.8 km/sec, and the fault slip is assumed to be uniform everywhere with a time history that is an isosceles triangle of 1-second duration. In Figure 7.10, I show the far-field time functions and the final response of individual rays as well as the total final vertical long-period P-waveforms for models that differ only in the location of their hypocenters. It is assumed that the motions are recorded by a long-period WWSSN seismometer (15-s seismometer, 100-s galvanometer).

An inspection of the synthetic seismograms in Figure 7.12 yields insight into the role of rupture on a finite fault. The difference in the durations of the far-field time functions for the individual rays is due to a **Doppler effect that is called directivity** by seismologists.
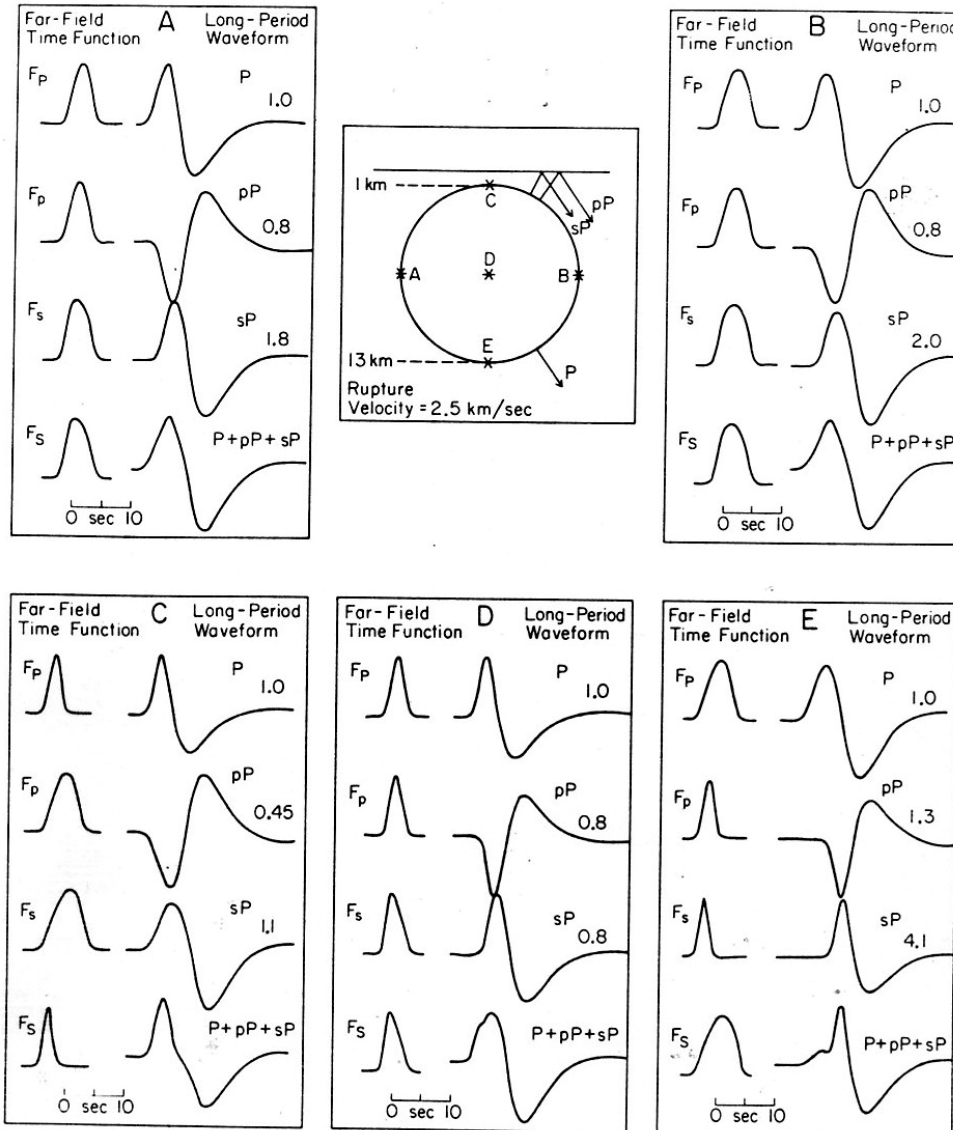
Figure 7.12. Illustration showing the effects of directivity on teleseismic P-waves from five earthquakes that are identical except for the location of their hypocenter. The ruptures are all on a circular, vertically-dipping strike-slip fault. F_P, F_p, F_s, and F_S, are the far-field time functions that are appropriate for the corresponding ray (see equation (7.59)). The seismograms on the right are those same time functions after convolving with a Q filter and an lon-period instrument response. The final seismograms are shown in the lower right. Notice that the effect of directivity is more important for hypocentral locations C (top of the fault) and E (bottom of the fault), since the P-waves leave the source region at near-vertical angles. The directivity effect is particularly evident when comparing F_S and F_s, since the rupture velocity is close to the shear wave velocity.

To provide insight into the solution to (7.54), I will begin with simple sources and then generalize to more complex sources. Let us first consider a **line source**. Of course, there are no true line sources in nature, but they demonstrate some important concepts in a simple way. Furthermore, they can be used to approximate ruptures whose along-strike length, L, is large compared to the down-dip width, w. For example, the 1906 San Francisco earthquake (M 7.8) has a rupture length of several hundred km and a width of less than 20 km.
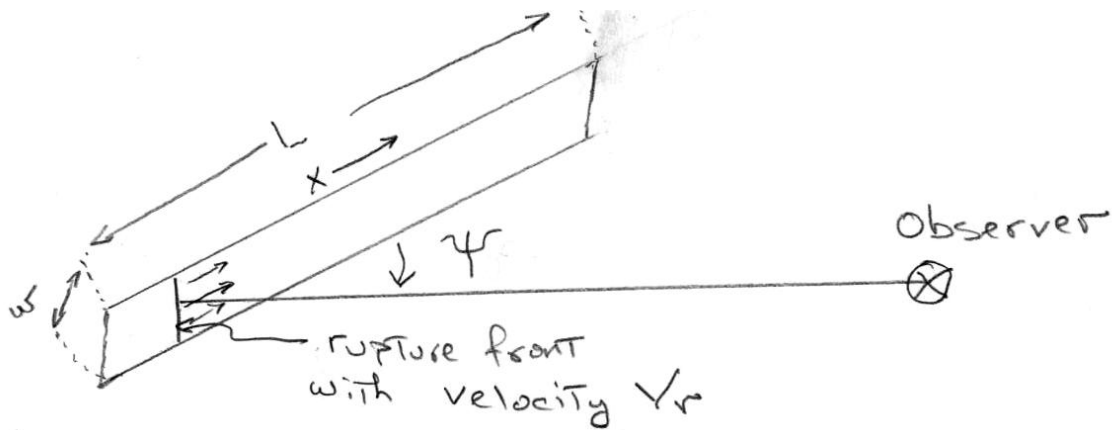
Figure 7.13. An idealized long and narrow fault.

To keep things simple, consider an observer in a homogeneous elastic whole space who is at a distance that is large compared to the fault length. Further consider the rupture geometry shown in Figure 7.13. The rupture is assume to be **unilateral,** which means that the rupture starts at one end and rupture to the other end. Some earthquakes rupture in both directions from the hypocenter and then they are called **bilateral**. Further assume that the slip at any point is given using a dimensionless along strike distance $\varsigma = \frac{x}{L}$.

$$D(\varsigma, t) = \bar{D}Lf(\varsigma)g\left(t - \frac{\varsigma L}{V_r}\right) \tag{7.65}$$

Where V_r is the rupture velocity, $\bar{D}$ is the average slip on the fault, $f(\varsigma)$ is a dimensionless function that describes the amplitude of the slip as a function of distance that is normalized by the average slip (i.e., $\int_0^1 f(\varsigma)d\varsigma = 1$,

$\int_0^1 D(\varsigma)d\varsigma = L\bar{D}$, and $g(t)$ is the time behavior of the slip at each point normalized

so that $\int_0^\infty g(t)dt = 1$. By writing slip on the fault in this way, we are assuming that the time dependences of the slip histories are the same for every point on the fault except for a delay due to the rupture velocity. While it is not really possible to decompose the slip history in this way, it is convenient for our purposes so that we can demonstrate several phenomena that appear in finite ruptures. Now let's assume that we are only interested in the far-field S-wave, since this is the wave that produces the largest particle velocities. Then for any point on our rupture, we can approximate the response from a Heaviside step in slip as (see equation (7.45))

$$G_\xi(x,t) = \frac{w(dx)\Re_\xi(\theta,\delta,\lambda,\phi,\zeta)}{4\pi} \frac{\delta\left(t - r(x)/\beta\right)}{\beta r(x)} * \frac{\partial H(t)}{\partial t}$$

$$= \frac{w(dx)\Re_\xi(\theta,\delta,\lambda,\phi,\zeta)}{4\pi} \frac{\delta\left(t - r(x)/\beta\right)}{\beta r(x)}$$

(7.66)

where $G_\xi(x,t)$ has units of displacement per unit slip, $\delta\left(t - r(x)/\beta\right)$ has units of inverse time, and where

$$r(x) \approx r_0(1 - x\cos\psi)$$

(7.67)

(7.66) and (7.67) can be written in terms of dimensionless along strike distance ς and $dx = Ld\varsigma$ as

$$G_\xi(\varsigma,t) = \frac{w(Ld\varsigma)\Re_\xi(\theta,\delta,\lambda,\phi,\zeta)}{4\pi} \frac{\delta\left(t - r(\varsigma)/\beta\right)}{\beta r(\varsigma)}$$

(7.68)

and

$$r(\varsigma) \approx r_0(1 - \varsigma L\cos\psi)$$

(7.69)

Since we are assuming an observer at a large distance, we assume that $\psi \approx \psi_0$, and we assume that the effect of distance on the amplitude (the r in the denominator) is negligible, and we can assume that the radiation pattern is approximately constant as a function of position along the rupture so that

$$G_\xi(x,t) \approx \frac{w(Ld\varsigma)\Re_\xi(\theta,\delta,\lambda,\phi_0,\zeta_0)}{4\pi} \frac{\delta\left(t - r_0(1 - L\varsigma\cos\psi_0)/\beta\right)}{\beta r_0}$$

(7.70)

Now we can write the response of the finite fault as

$$u(t) = \int_0^1 \bar{D} f(\varsigma) \dot{g}\left(t - \frac{\varsigma L}{V_r}\right) * G_\xi(\varsigma, t)(L d\varsigma)$$

$$= \int_0^1 \left[\bar{D} f(\varsigma) \dot{g}\left(t - \varsigma L/V_r\right) * \frac{w\Re_\xi}{4\pi\beta r_0} \delta\left(t - r_0/\beta + \varsigma L \cos\psi_0/\beta\right) \right](L d\varsigma)$$

$$= \frac{wL\bar{D}\Re_\xi}{4\pi\beta r_0} \dot{g}\left(t - r_0/\beta\right) * \int_0^1 f(\varsigma)\delta\left(t + \varsigma L \cos\psi_0/\beta - \varsigma L/V_r\right) d\varsigma \qquad (7.71)$$

$$= \frac{wL\bar{D}\Re_\xi}{4\pi\beta r_0} \dot{g}\left(t - r_0/\beta\right) * \int_0^1 f(\varsigma)\delta(t - \varsigma T) d\varsigma$$

$$= \frac{wL\bar{D}\Re_\xi}{4\pi\beta r_0} \dot{g}\left(t - r_0/\beta\right) * f\left(\frac{t}{T}\right)$$

where

$$T = L\left(\frac{1}{V_r} - \frac{\cos\psi_0}{\beta}\right) = \frac{L}{\beta}\left(\frac{\beta}{V_r} - \cos\psi_0\right) \qquad (7.72)$$

T is actually the difference in shear-wave arrival times from a point at the hypocenter $(x = 0)$ and a point at the end of the rupture $(x = L)$, including the time it takes the rupture to get from one end of the fault to the other.

Equation (7.71) tells us that if the rupture velocity is constant on a line source, then the ground displacement from the far-field shear-wave is the same function of time $f\left(t/T\right)$ that the slip was as a function of distance along the fault $f\left(x/L\right)$ (see equation (7.65)), but with an amplitude that is scaled by the $1/T$. In Figure 7.14, I show how the far-field S-wave displacement depends on receiver location, assuming that the slip at each point is instantaneous (i.e., assuming that $g(t) = H(t)$). Notice that the area under the pulse is identical for every receiver, except for the radiation pattern and the geometric spreading. This solution tells us that spatial variations in slip map into temporal variations in the seismic waves.
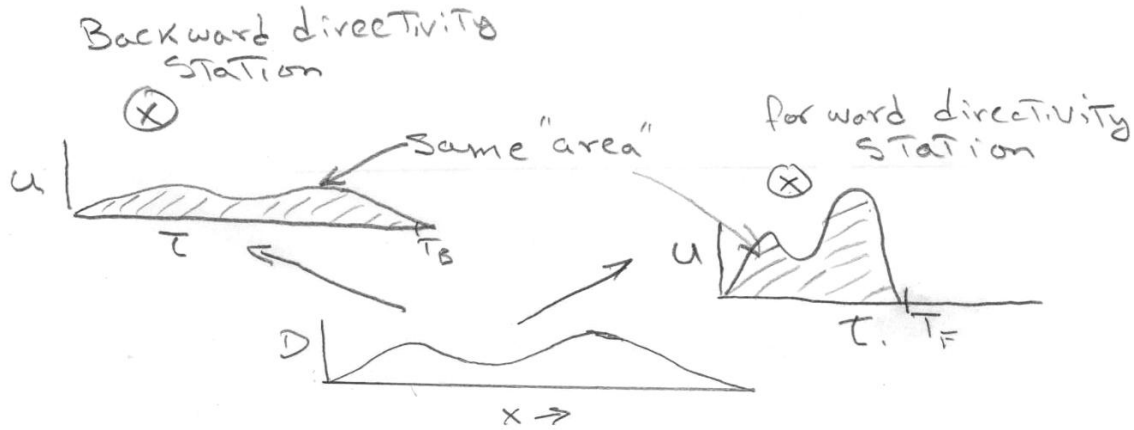
Figure 7.14. Schematic showing the relationship between the far-filed S-wave displacement time history and the spatial variation in slip along a line source in which the rupture proceeds from left to right at a constant velocity. The slip is considered to be a Heaviside function with time. Notice that the temporal variation of the far-field S-wave is identical to the spatial variation in the slip, except for a time contraction factor. This time contraction factor is specified by the time difference between the arrival of S-waves from each end of the fault.

If the slip at each point on the fault is very short (approximately a step function), and if you know the rupture velocity and fault geometry, the equation (7.71) tells us that we can derive the along-strike slip amplitude by a simple deconvolution process. Of course, we do not a priori know the rupture velocity and the duration of slip at each point. However, if we know the far-field S-wave at several stations then we can simultaneously determine $f\left(\dfrac{x}{L}\right)$, $g(t)$, and V_r.

I won't go through the derivation here, but it can be shown that spatial variations in the rupture velocity also map into temporal variations in the far-field S-wave displacement. That is, complexity in the far-field S-wave can be caused by either spatial complexity in the amplitude of the slip, or in complexity in the rupture velocity.

At this point, it is useful to look at the characteristics of seismic waves that are produced if the slip on the fault is assumed to be spatially uniform, that is assume that

$$f\left(\frac{x}{L}\right) = \Pi\left(\frac{x}{L}\right) \equiv \begin{cases} 0 & x < 0 \\ \dfrac{1}{L} & 0 < x < L \\ 0 & x > L \end{cases} \qquad (7.73)$$

In this case equation (7.71) becomes

$$u(t) = \frac{wL\bar{D}\mathfrak{R}_\xi}{4\pi\beta r_0}\,\dot{g}\!\left(t - \frac{r_0}{\beta}\right) * \Pi\!\left(\frac{t}{T}\right) \tag{7.74}$$

We can now enquire about the energy flux of a radiated far-field shear wave through a patch of area $r_0^2 d\phi d\zeta$. We obtain this by integrating the energy flux per unit area $P = \rho\beta\dot{u}^2$ with respect to time (see equation 3.51). In this case

$$
\begin{aligned}
E &= r_0^2 d\phi d\zeta \int_0^\infty \rho\beta \left[\frac{wL\bar{D}\mathfrak{R}_\xi}{4\pi\beta r_0}\,\dot{g}\!\left(t - \frac{r_0}{\beta}\right) * \dot{\Pi}\!\left(\frac{t}{T}\right)\right]^2 dt \\
&= \rho d\phi d\zeta \frac{1}{\beta}\left(\frac{wL\bar{D}\mathfrak{R}_\xi}{4\pi}\right)^2 \int_0^\infty \left[\dot{g}\!\left(t - \frac{r_0}{\beta}\right) * \frac{\delta(t) - \delta(t-T)}{T}\right]^2 dt \\
&= \rho d\phi d\zeta \frac{1}{\beta}\left(\frac{wL\bar{D}\mathfrak{R}_\xi}{4\pi}\right)^2 \frac{1}{T^2}\int_0^\infty \left[\dot{g}(t) - \dot{g}(t-T)\right]^2 dt
\end{aligned} \tag{7.75}
$$

At this point we see that the density of radiated energy depends strongly on the duration of the far-field S-wave T. In order to evaluate (7.75), we will assume that the slip at every point is a ramp of duration τ_r, which is usually called either the "rise time" or the "slip duration." That is assume that

$$g(t) = \Pi\!\left(\frac{t}{\tau_r}\right) \equiv \begin{cases} 0 & t < 0 \\ \frac{t}{\tau_r} & 0 < t < \tau_r \\ 1 & t > \tau_r \end{cases} \tag{7.76}$$

In this case,

$$\dot{g}(t) - \dot{g}(t-T) = \frac{1}{\tau_r}\left[H(t) - H(t - \tau_r)\right] - \left[H(t-T) - H(t - T - \tau_r)\right] \tag{7.77}$$

There are two cases to consider; i) $\tau_r < T$, and ii) $\tau_r > T$. The first case, $\tau_r < T$, corresponds to a case in which the duration of slip is short compared to the rupture time. This type of rupture model is often referred to as a Haskell-like model (Haskell, 1964, BSSA, 1811-1841) and it has sometimes been criticized since the slipping at any point on the fault arrest without any inherent knowledge of the ends of the rupture. However, more recent work suggest that rupture may propagate as a solitary wave of slip that is called a slip pulse (also sometimes referred to as a Heaton pulse, Heaton, T.H., 1990 Evidence for and implications of self-healing pulses of slip in earthquake rupture, *Phys. Earth Planet Int.*, *Vol 64.* 1-20). The second case $\tau_r > T$ has rupture durations that are longer than the rupture time and they are referred to as "crack-like" models since the amplitude and duration of the slip are controlled by the dimension of the rupture. We will come back to further discuss these two models later in Chapter 8. Figure 7.15 shows a sketch of $\dot{g}(t) - \dot{g}(t-T)$ for these two cases.
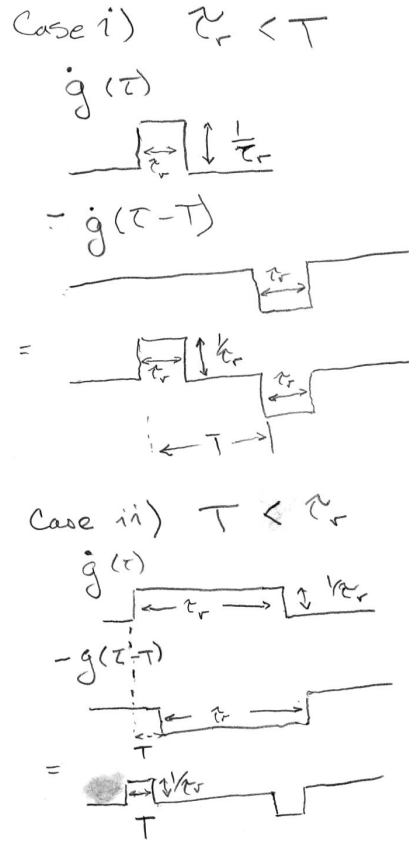
Figure 7.15 Schematic showing $\dot{g}(t) - \dot{g}(t-T)$, which is used for evaluating energy in equation (7.75) for a slip pulse model (case i) and for a crack-like model (case ii).

Let's first see what happens for the slip pulse model (case i).

$$E = \rho d\phi d\zeta \frac{1}{\beta} \left(\frac{wL\bar{D}\Re_\xi}{4\pi} \right)^2 \frac{1}{T^2} \int_0^\infty \left[\dot{g}(t) - \dot{g}(t-T) \right]^2 dt$$

$$= \rho d\phi d\zeta \frac{1}{\beta} \left(\frac{wL\bar{D}\Re_\xi}{4\pi} \right)^2 \frac{1}{T^2} \int_0^\infty \left[\Pi\left(\frac{t}{\tau_r} \right) - \Pi\left(\frac{t}{\tau_r} - T \right) \right]^2 dt$$

$$= \rho d\phi d\zeta \frac{1}{\beta} \left(\frac{wL\bar{D}\Re_\xi}{4\pi} \right)^2 \frac{1}{T^2} \int_0^\infty \left[\Pi^2\left(\frac{t}{\tau_r} \right) + \Pi^2\left(\frac{t}{\tau_r} - T \right) \right] dt \qquad (7.78)$$

$$= \rho d\phi d\zeta \frac{1}{\beta} \left(\frac{wL\bar{D}\Re_\xi}{4\pi} \right)^2 \frac{1}{T^2} \int_0^\infty 2\Pi^2\left(\frac{t}{\tau_r} \right) dt$$

$$= 2\rho d\phi d\zeta \frac{1}{\beta} \left(\frac{wL\bar{D}\Re_\xi}{4\pi} \right)^2 \frac{1}{T^2} \frac{1}{\tau_r}$$

We see that the radiated energy flux is very sensitive to T and τ_r. We can substitute (7.72) into (7.78) to obtain

$$E = 2\rho d\phi d\zeta \left(\frac{w\bar{D}\Re_\xi}{4\pi}\right)^2 \frac{1}{\tau_r} \frac{\beta}{\left(\dfrac{\beta}{V_r} - \cos\psi_0\right)^2} \tag{7.79}$$

Notice that the length of the fault drops out of this expression. This is because the only part of the radiated far-field S-wave is from the beginning of the rupture (a starting phase) and the end of the rupture (a stopping phase). As we have noted before, **there is no far-field radiation from a rupture that is propagating in a steady state.** Of course this does not mean that there is no motion in the medium, it just means that the far-field terms (which comprise the radiated energy) are zero. The rest of the motion is comprised of the near-field terms.

We can now evaluate our crack-like model (case ii) in a similar way to obtain

$$E = \rho d\phi d\zeta \frac{1}{\beta}\left(\frac{wL\bar{D}\Re_\xi}{4\pi}\right)^2 \frac{1}{T^2}\int_0^\infty \left[\dot{g}(t) - \dot{g}(t-T)\right]^2 dt$$

$$= \rho d\phi d\zeta \frac{1}{\beta}\left(\frac{wL\bar{D}\Re_\xi}{4\pi}\right)^2 \frac{1}{T^2}\int_0^\infty \left[\Pi\left(\frac{t}{T}\right)\frac{T}{\tau_r} - \Pi\left(\frac{t}{T} - \tau_r\right)\frac{T}{\tau_r}\right]^2 dt$$

$$= \rho d\phi d\zeta \frac{1}{\beta}\left(\frac{wL\bar{D}\Re_\xi}{4\pi}\right)^2 \frac{1}{T^2}\int_0^\infty 2\left(\frac{T}{\tau_r}\right)^2 \Pi^2\left(\frac{t}{\tau_r}\right) dt$$

$$= 2\rho d\phi d\zeta \frac{1}{\beta}\left(\frac{wL\bar{D}\Re_\xi}{4\pi}\right)^2 \frac{1}{T}\frac{1}{\tau_r^2} \tag{7.80}$$

As before we can substitute (7.72) into (7.80) to obtain

$$= 2\rho d\phi d\zeta \left(\frac{wL\bar{D}\Re_\xi}{4\pi}\right)^2 \frac{1}{L\left(\dfrac{\beta}{V_r} - \cos\psi_0\right)} \frac{1}{\tau_r^2} \tag{7.81}$$

Notice that fault length is back in the expression, and that the radiated energy becomes very small as the rise time becomes large. In general, pulse-like ruptures radiate far more energy than do crack-like ruptures given the same fault dimensions and slip (that is the same potency).

Static Offsets from Finite Faults

The last section covered the problem of radiated waves, that is, they obey the homogeneous form of Navier's equation. However, there are other important terms to the solution for ground motions close to a finite rupture. Although it is common to use the word "near-field" for any site close to a rupture, I personally like to reserve the word "near field" to refer to the non-radiated parts of the

solution. I suggest using the word "near-source" when the observer is close to a fault. Of course, the definition of close is subjective, but generally speaking it refers to sites that are less than a fault width away from the rupture (assuming that rupture width is the shorter of the two principal axes that span the rupture surface). As mentioned earlier, there are several types of near-field terms (see Figure 7.4), but the combination of terms that comprise the static solution are generally the most important.

Chinnery (The deformation of the ground around surface faults, Bull. Seism. Soc. Am., 1961, v. 51, 355-372) described the static solution for a rectangular strike-slip finite fault in a homogenous half-space with uniform slip. Figure 7.16 shows the geometry of the fault. Please not that the notation is different here; D is the bottom depth of the fault and not the fault slip.   Figure 7.17 schematically shows the displacements (in units of 10^{-3} times the fault slip) at the free surface assuming a fault that extends to the surface, i) and a bottom depth of 0.1 times L, and ii) a bottom depth that is 2.0 times L (a square fault). The motion right at the fault surface is symmetric about the fault plane and it is ½ of the fault slip, which would correspond to a contour of 500. This contour is not seen in the plots since this only occurs right at the fault. If d=0, L>>y1, y2, and D, then

$$u_1 \approx \frac{U}{\pi} \tan^{-1} \frac{D}{y_2}$$

$$u_2 \approx u_3 \approx 0$$

(7.82)

By fitting (7.82) to geodetic data close to fault slips, we can approximately determine the bottom depth of slip. At distances that are large compared to the fault dimensions, the source can be approximated as a point-source, and the amplitude of the static displacements then decrease as R^{-2}. Coincidentally, since strain is proportional to spatial derivatives of displacement, the static change in strain (and also stress) decreases as R^{-3} when the distance is large compared to the rupture dimension.
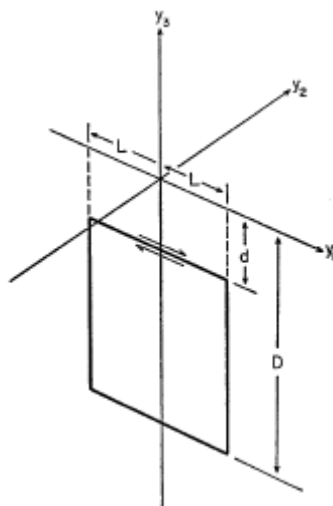

Figure 7.16. Chinnery's (1961) description of a vertical strike-slip fault embedded in an elastic half space.
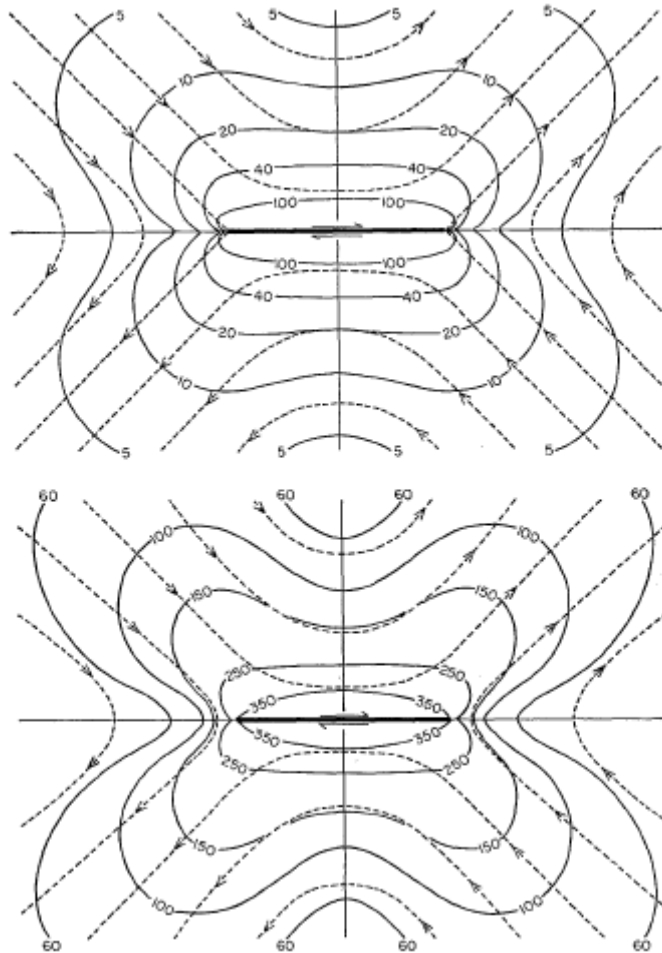
Figure 7.17. Map of the static displacement vectors from a vertical
strike-slip fault with uniform slip that extends to the earth's surface
and as observed at the free surface. The directions of the
displacement vectors are parallel to the dotted lines and in the
direction of the arrows. The contours give the amplitude of the
vectors in units of 10^{-3} times the uniform slip assumed on the fault.
The top panel shows a fault with a width that is 5% of its length
and the bottom panel shows a fault with a width that is equal to its
length.

Because of the symmetries in Chinnery's problem, the static deformation for a
vertical strike-slip fault that extends to the surface of a half space is the same
solution as for a vertical fault in a whole space, but with the width of the fault
doubled. The problem becomes a little more complex for a dipping fault in a
homogeneous half-space. Mansinha and Smylie (1971, The displacement fields of
inclined faults, Bull. Seism. Soc. Am., 61, 1433-1440) presented the closed-form
solution for a uniform slip on a dipping fault in a half-space. Figure 7.18 shows the
geometry of the fault that they assumed. Figure 7.19 shows the displacements at
the free surface along a line that is perpendicular to the fault strike and that bisects
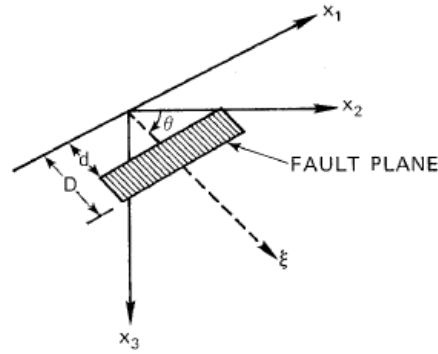
Figure 7.18. Mansiha and Smylie (1971) derived the static displacement field caused by a uniform slip on a dipping fault in an elastic half space.
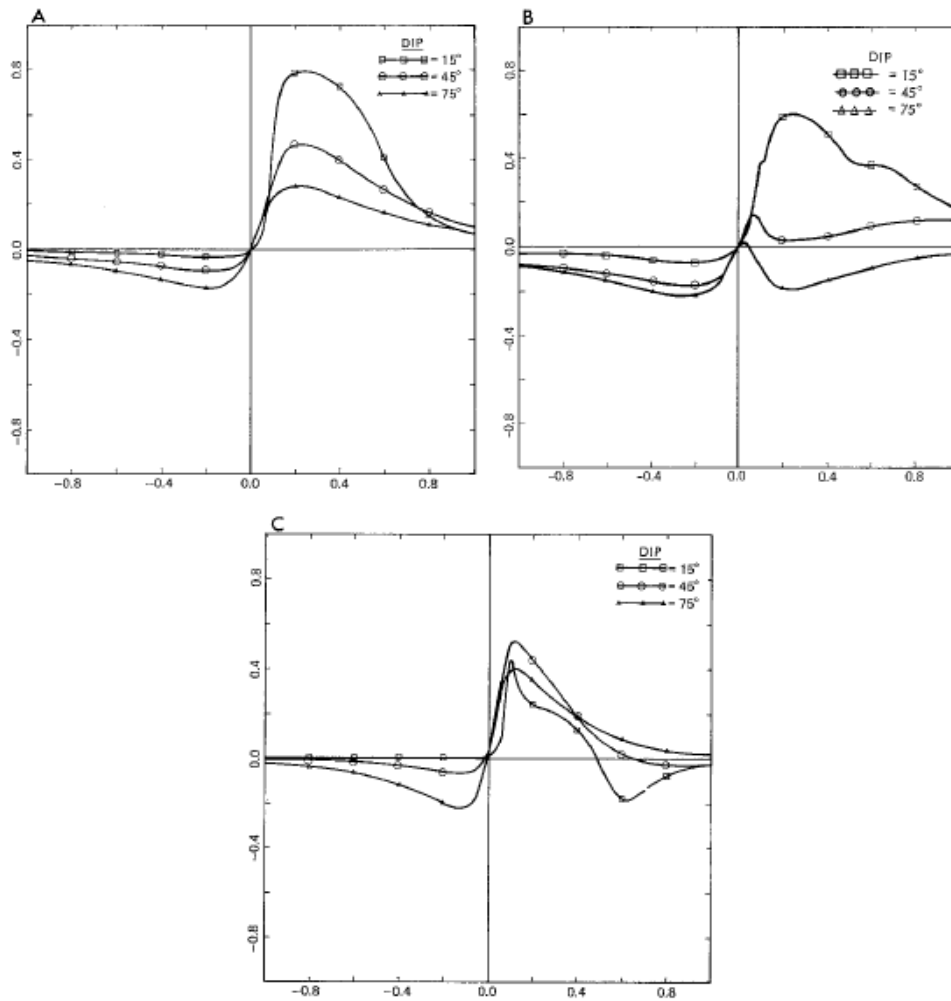

Figure 7.19. (from Mansinha and Smylie, 1971). Static ground displacements (one unit is fault offset) as a function of distance along the axis x2 (line perpendicular to the fault strike) where one unit is L, and the fault length is 2L. Panel A is fault parallel motion from a dipping fault with strike slip motion. Panel B is fault-perpendicular horizontal motion for with dip-slip motion. Panel B is vertical motion for dip-slip motion.

the middle of the fault. Panel A is horizontal fault-strike-parallel static motion for a dipping fault with strike-slip motion (the other components of motion are identically zero along this line). Panel B is horizontal fault-strike-perpendicular motion for a dipping fault with dip-slip motion. Panel C is the vertical motion for a dipping fault with dip-slip motion.